# Calculation of Water Collection Efficiency Using a Multiphase Flow Solver

Yisen Guo* and Yongsheng Lian†
*University of Louisville, Louisville, Kentucky 40292*

DOI: 10.2514/1.C034793

**This paper reports a new method to calculate water collection efficiency. The method is based on a well-validated multiphase flow solver that solves the Navier–Stokes equations using the projection method on Cartesian grids and uses the moment-of-fluid method to construct the interfaces between different phases. The numerical method is validated against experimental results with good agreement. Using this method, the water collection efficiency of an MS(1)-317 wing is investigated. The current simulations show that the proposed method gives a better prediction of water collection efficiency when large drops are involved. The prediction is attributed to the better modeling of drop and airflow interaction, as well as the consideration of drop splashing.**



## Nomenclature

| | | |
|---|---|---|
| $C_D$ | = | drag coefficient |
| $C_L$ | = | lift coefficient |
| $c$ | = | airfoil cord length, m |
| $D_0$ | = | initial drop diameter, m |
| $h$ | = | liquid film thickness, m |
| $K$ | = | dimensionless splashing parameter |
| $Oh$ | = | Ohnesorge number |
| $Re$ | = | Reynolds number |
| $V_0$ | = | impact velocity, m/s |
| $We$ | = | Weber number |
| $\alpha$ | = | angle of attack, deg |
| $\beta$ | = | water collection efficiency |
| $\delta$ | = | dimensionless liquid film thickness |
| $\theta$ | = | contact angle, deg |
| $\mu_a$ | = | viscosity of air, kg/(m · s) |
| $\mu_w$ | = | viscosity of water, kg/(m · s) |
| $\rho_a$ | = | density of air, kg/m$^3$ |
| $\rho_w$ | = | density of water, kg/m$^3$ |
| $\sigma_{as}$ | = | air/solid surface tension, N/m |
| $\sigma_{wa}$ | = | water/air surface tension, N/m |
| $\sigma_{ws}$ | = | water/solid surface tension, N/m |

## I. Introduction

### A. Water Collection Efficiency and Its Importance

AIRCRAFT icing under extreme weather conditions is one of the major serious hazards to affect aviation safety. Ice accretion on the external parts of an aircraft during flight is caused by freezing rain/drizzle or supercooled water drops. Icing on aircraft could alter the effective wing geometry and impact the performance and control of the aircraft [1,2]. Therefore, performing an aircraft icing analysis is crucial for assessing the effect of ice accretion on an aircraft. One important stage in an aircraft icing analysis is to determine the water collection efficiency and impact limit.

The local water collection efficiency $\beta$ is defined as the volume flux ratio of an infinitesimal area with water drops $dA_\infty$ to the corresponding impingement area on the airfoil $dA$ by using the drop trajectory data [3]. As shown in Fig. 1, the local water collection efficiency $\beta$ can be expressed as follows:

$$\beta = \frac{dA_\infty}{dA} \tag{1}$$

Because water drops can splash after impact on the surface, the local water collection efficiency is modified with the consideration of the drop splashing phenomenon and is expressed as follows:

$$\beta_{\text{splash}} = \frac{dA_\infty}{dA}\left(\frac{\dot{m}_{\text{splash}}}{\dot{m}_{\text{film}} + \dot{m}_{\text{splash}}}\right) \tag{2}$$

where $\dot{m}_{\text{film}}$ denotes the mass depositing onto the surface, and $\dot{m}_{\text{splash}}$ denotes the mass loss due to splashing. The impact limit is defined as the upper and lower limits that water drops can impinge on the surface. Deicing devices are required within the impact limit to remove ice. Experiments have shown that airspeed, drop size, airfoil type, and body size are primary parameters for determining the water collection efficiency and impact limit [4–6].

### B. Existing Methods to Predict Water Collection Efficiency

Various approaches have been proposed to obtain the local water collection efficiency. Experimental studies were started in the early 1950s, and dyed water drops were sprayed onto the surface of a body covered with absorbent blotting paper [6–8]. The local collection efficiency was obtained using a laser reflectance spectroscopy method by analyzing the amount of dye on the blotter paper in a given time interval.

Numerical studies are also conducted to investigate the local collection efficiency and ice accretion, and different models have been proposed and developed. Most of these models sequentially solve different sets of equations to obtain airflow, drop trajectory and impingement, heat transfer, and phase change to study aircraft ice accretion. Among them, FENSAP-ICE, initially proposed by Bourgault et al. [9,10], uses an Eulerian approach to account for water drop impingement. FENSAP-ICE solves the liquid phase independent of the gas phase; therefore, the water drops do not affect the airflow. This method is validated by successfully predicting the local collection efficiency of small water drops. LEWICE [11–13] (which stands for the Lewis ice accretion program) is the main icing code used in the United States and was developed by NASA John H. Glenn Research Center. LEWICE uses a panel method combined with a Lagrangian drop trajectory method to determine collection efficiency. The drop is assumed to be a rigid sphere and does not affect the airflow. LEWICE also has the capability to use Navier–Stokes methods for airflow. Drop breakup and splashing are considered in LEWICE for calculating the local collection efficiency, and good agreement is achieved with experimental data. ONICE2D (which stands for the ONERA two-dimensional icing suite) [14] uses a Lagrangian approach to calculate the deposition probability of each drop, and then it determines whether the drop fully deposits on the solid surface or collides with secondary drops from previous drop

Received 17 October 2017; revision received 14 September 2018; accepted for publication 26 September 2018; published online 7 December 2018. 

*Ph.D. Student, Department of Mechanical Engineering.
†Associate Professor, Department of Mechanical Engineering.

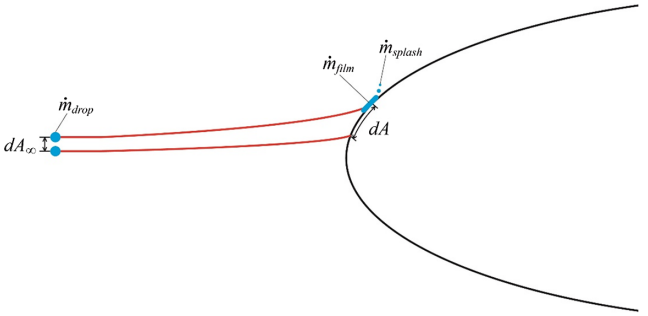


**Fig. 1 Definition of water collection efficiency [3].**

impacts. ONICE2D also considers the effect of drop shape on drag force when calculating trajectory. Table 1 lists some existing models for calculating water collection efficiency and their approaches [9–14,16–18]. Most of the models consider the effect of air flow on the drop (the drag and the trajectory), but the effect of the drop on the flowfield is largely ignored. Drop splashing has a significant effect on the water collection efficiency. However, most studies either ignore drop splashing or are based on simplified empirical splashing models [15].

### C. Effect of Large Drops on Water Collection Efficiency

Drop may splash when it impinges on a surface at a high speed, and splashing is an important phenomenon for supercooled large drops (SLDs). A SLD usually refers to a liquid drop with diameter larger than 50 $\mu$m. SLDs remain in liquid form even when the temperature is below the freezing point because of the lack of freezing nuclei. Aircraft icing under SLD conditions imposes great danger to aviation safety and has been recognized as a significant aviation hazard [11,19]. Several fatal aviation accidents have been caused by SLDs, and recent studies indicated icing due to SLDs occurred more frequently than initially realized [20,21]. Icing due to SLD conditions has been extensively studied in recent years and has been included in the regulations of the Federal Aviation Administration [22] and the European Aviation Safety Agency [23].

Due to its large size, a SLD can splash into secondary drops when it impacts a surface, which reduces the amount of water depositing onto the surface and accordingly affects the local collection efficiency significantly. Besides, the splashed drops can reimpinge onto unprotected surfaces to form ice [20]. Therefore, accurately predicting the splashing physics and mass loss is crucial in calculating local collection efficiency. However, the underlying mechanism of large drop splashing is still not fully understood [13,24,25].

In this paper, we take an integrated Eulerian approach to study the water collection efficiency and impingement limit using a multiphase flow solver. In this approach, we solve the Navier–Stokes equations and use the moment of fluid method to represent the interfaces. Unlike most previous methods, our approach considers the interplay between air and drops. The drop deformation and impingement on the wing surface and its subsequent behaviors are captured.

## II. Numerical Methods

The numerical method was discussed in detail in earlier papers by Li et al. [26], Guo et al. [27], and Guo and Lian [28]. Here, we briefly present the key steps with an emphasis on interface reconstruction when more than two materials exist.

### A. Governing Equations

The governing equations for incompressible, immiscible, multiphase flows are

$$\nabla \cdot \boldsymbol{U} = 0 \tag{3}$$

$$\frac{\partial \rho \boldsymbol{U}}{\partial t} + \nabla \cdot (\rho \boldsymbol{U} \otimes \boldsymbol{U}) = -\nabla p + \nabla \cdot (2\mu D) + \rho \boldsymbol{g} - \sum_{m=1}^{M} \gamma_m \kappa_m \nabla H(\phi_m) \tag{4}$$

$$\frac{\partial \phi_m}{\partial t} + \boldsymbol{U} \cdot \nabla \phi_m = 0 \qquad m = 1, \cdots, M \tag{5}$$

where $\boldsymbol{U} = (u, v, w)$ is the velocity vector, $t$ is the time, $p$ is the pressure for material, $\boldsymbol{g}$ is the gravitational acceleration vector, and $D$ is the rate of deformation tensor:

$$D = \frac{\nabla \boldsymbol{U} + (\nabla \boldsymbol{U})^T}{2} \tag{6}$$

Here,

$$\mu \equiv \sum_{m=1}^{M} \mu_m H(\phi_m)$$

is the viscosity. $H$ is the Heaviside function defined as

$$H(\phi) = \begin{cases} 1 & \phi \geq 0 \\ 0 & \text{otherwise} \end{cases} \tag{7}$$

The stress at the material interface will have the following jump condition:

$$[(-pI + 2\mu D) \cdot \boldsymbol{n}] = \sigma \kappa \boldsymbol{n} \tag{8}$$

where $\sigma$ is the surface tension coefficient, and $\kappa$ and $\boldsymbol{n}$ are the curvature and unit normal of the interface, respectively. The interface unit normal is

$$\boldsymbol{n} = \frac{\nabla H}{|\nabla H|} \tag{9}$$

Also, $\phi_m$ is the level set function for material m and satisfies

$$\phi_m(\boldsymbol{x}, t) = \begin{cases} > 0 & \boldsymbol{x} \in \text{material } m \\ \leq 0 & \text{otherwise} \end{cases} \tag{10}$$

**Table 1 Selected existing models for calculating water collection efficiency**

| | Lagrangian or Eulerian | Airflow | Interaction between drops and airflow | Drop deformation | Drag model | Drop splashing |
|---|---|---|---|---|---|---|
| LEWICE [11–13] | Lagrangian | Panel method | Drops do not affect airflow | No | Drag for spheres | Yes |
| FENSAP-ICE [9,10] | Eulerian | Euler or Navier–Stokes solver | Drops do not affect airflow | No | Shiller–Naumann drag model | No |
| ONICE2D [14] | Lagrangian | Panel method | Drops do not affect airflow | Yes | Shiller–Naumann drag model | Yes |
| CANICE [16] | Lagrangian | Panel method | Drops do not affect airflow | No | — — | No |
| TURBICE [17] | Lagrangian | Panel method | Drops do not affect airflow | No | — — | No |
| Da Silveira et al. [18] | Eulerian | Navier–Stokes solver | Mutual interaction | No | Drag coefficients for spherical and nonspherical particles | No |

### B. Moment of Fluid Interface Reconstruction

The moment of fluid (MOF) method [29–33] is used to reconstruct the phase interfaces. In the MOF method, we represent the material $m$ distribution using its volume fraction and centroid. In each computational cell $\Omega_{i,j,k}$, the volume fraction of material $m$ is the zeroth-order moment

$$F_m = \frac{1}{|\Omega_{i,j,k}|}\int_{\Omega_{i,j,k}} H(\phi_m(\boldsymbol{x}))\,\mathrm{d}\boldsymbol{x} \tag{11}$$

and the centroid of the material is the first-order moment

$$\boldsymbol{x}_m = \frac{\int_{\Omega_{i,j,k}} H(\phi_m(\boldsymbol{x}))\boldsymbol{x}\,\mathrm{d}\boldsymbol{x}}{\int_{\Omega_{i,j,k}} H(\phi_m(\boldsymbol{x}))\,\mathrm{d}\boldsymbol{x}} \tag{12}$$

In each computational cell, the interface between different phases is represented by a plane in a three-dimensional grid or a line in a two-dimensional grid, which is called the piecewise linear interface calculation. For the two-dimensional grid, the interface can be represented by a straight line as shown in Fig. 2 using the following equation:

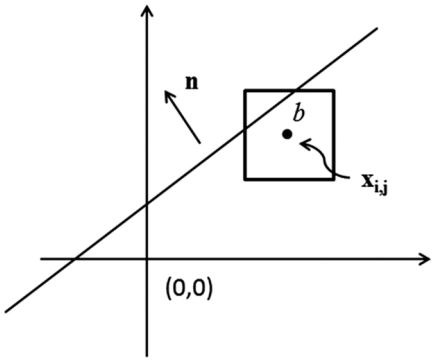


**Fig. 2 Interface represented by a straight line in the two-dimensional case. The square represents a computational cell.**

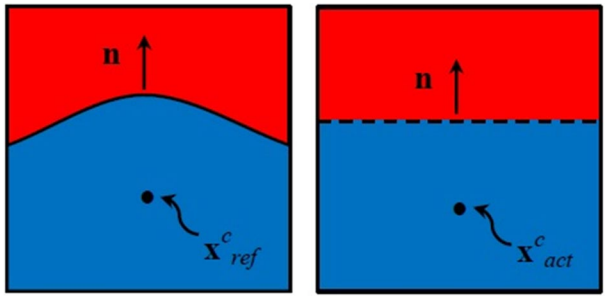


**Fig. 3 MOF interface reconstruction. The solid curved line represents the true interface, and the dashed straight line represents the reconstructed interface.**

$$\boldsymbol{n}\cdot(\boldsymbol{x}-\boldsymbol{x}_{i,j}) + b = 0 \tag{13}$$

where $\boldsymbol{n}$ is the unit normal vector, $\boldsymbol{x}_{i,j}$ is the cell center, and $b$ is the distance from the cell center to the line.

The MOF method uses both the volume fraction function of $F_m = F_m(\boldsymbol{n}, b)$ and the corresponding material centroid of $\boldsymbol{x}^c_m = \boldsymbol{x}^c_m(\boldsymbol{n}, b)$ to construct the interface. Given a reference volume fraction function $F_{\mathrm{ref},m}$ and a reference centroid $\boldsymbol{x}^c_{\mathrm{ref},m}$ in one computational cell, the MOF interface reconstruction requires that the actual volume fraction function matches the reference volume fraction function exactly and that the actual centroid is close to the reference centroid as illustrated in Fig. 3.

This procedure can be achieved by following the constraint optimization problem:

$$E_{\mathrm{MOF}} = \|\boldsymbol{x}^c_{\mathrm{ref},m} - \boldsymbol{x}^c_{\mathrm{act},m}(\boldsymbol{n}, b)\|^2$$
$$\text{subject to } |F_{\mathrm{ref},m} - F_{\mathrm{act},m}(\boldsymbol{n}, b)| = 0 \tag{14}$$

The step-by-step procedure was described by Jemison et al. [34].

Adaptive mesh refinement is used to the reduce computation cost [35,36]. As shown in Fig. 4, the mesh refinement is near the liquid/air interfaces. Two or three levels of refinement are used in most of the reported work here.

### C. Procedure of Calculating Water Collection Efficiency

The calculation of water collection efficiency is done through a two-step process. In the first step, the efficiency is calculated based on the drop trajectory without considering the drop splashing. In the second step, the efficiency is adjusted based on the output of splashing. The procedure is shown in Fig. 5. In the first step, we calculate the drop trajectories based on the size group and use a seven-bin drop distribution to represent the median volume diameter (MVD). In our simulation, we position a group of drops of the same size in front of the sphere and assign them the same velocity as the surrounding air. The simulation is then first conducted to obtain the trajectory of each drop. The water collection efficiency based on the area ratio is calculated according to Eq. (1): the spacing between drops at the initial upstream location is $dA_\infty$, the corresponding spacing between impinged drops on the airfoil is $dA$, and the local collection efficiency $\beta_i$ is the ratio between $dA_\infty$ and $dA$. For any drop that eventually hits the solid surface, its terminal speed and impact angle right before hitting the airfoil are then recorded. To determine the impingement limit, the simulation is rerun with more drops in the region in which one drop impacts the surface while the neighboring drop misses in the initial run. A separated simulation with fine mesh is used to calculate the volume of the splashed drops of these drops based on the recorded terminal speed and impact angle. The water collection efficiency is then adjusted based on the splashed volume. These steps repeat until all groups are evaluated.

## III. Results and Discussion

We first validate our code by comparing with the experimental results. Then, we study the high-speed drop impact on a dry surface and on a wet surface at the conditions pertinent to aircraft icing. Last, we study the water collection efficiency of a sphere and an MS(1)-317

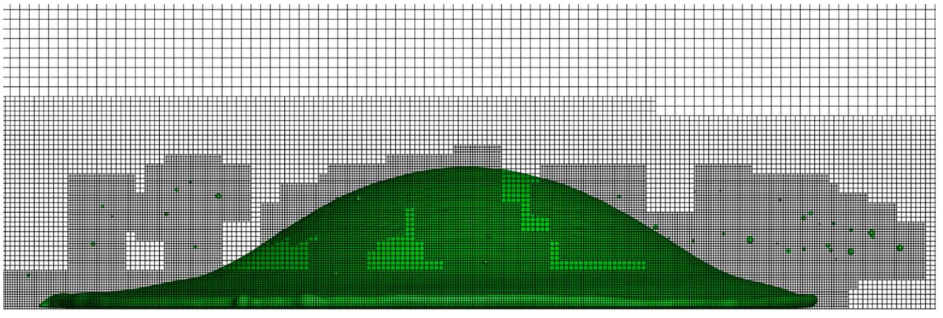

**Fig. 4 Two-level adaptive mesh refinement in the simulation of the drop impact on a dry solid substrate. Grid refinement is near the interfaces.**

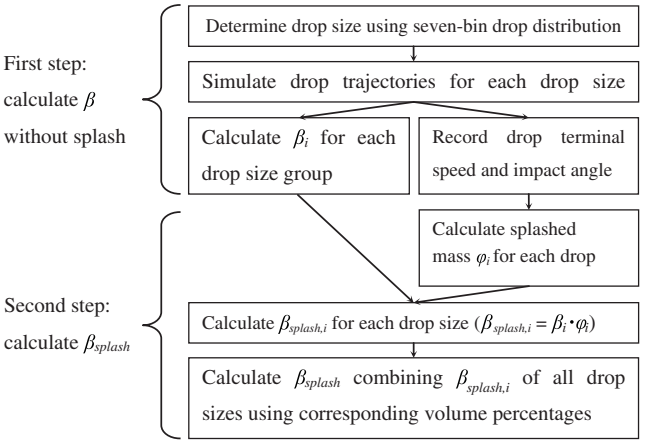


**Fig. 5 Procedure of calculating water collection efficiency.**

airfoil. In all simulations, we assume the water is at room temperature and there is a static contact angle of 70 deg. A dynamic contact angle model of Jiang et al. [37] is used to model the dynamic change of the contact angle with the contact line velocity.

### A. Code Validation: Drop Impact on Dry Surface

Mundo et al. [38] experimentally studied drop impingement onto a rotating disk and performed a statistical analysis of the splashed secondary drops. The normal impact velocity of the drop and the tangential velocity of the rotating disk led to oblique impact. They concluded that the normal velocity component determined the size distribution of the secondary drops. To validate our code, we select one case from their study to simulate. The size and velocity distributions of the splashed drops are then analyzed and compared with their experimental results. Because those splashed drops have irregular shapes, we use an equivalent drop diameter, which makes a sphere have the same volume as an irregular drop. The velocity of each splashed secondary drop is the mass-averaged velocity. The shooting angle is the angle between the bouncing velocity vector and the tangent direction of the solid surface at the location of bouncing.

The experiment uses a solid dry surface. The initial diameter of the drop $D_0$ is 100 $\mu$m; the impingement velocity is 15 m/s; and the impingement angle $\alpha$ is 37 deg, leading to a normal impact velocity $V_0$ of 12 m/s. The liquid viscosity is 2.76 mPa · s, and the surface tension is 22 mN/m. The resulting Reynolds number $Re$ is 1182 and Weber number $We$ is 868. Note that both the Reynolds number $Re$ and the Weber number $We$ are calculated using the normal impact velocity. The resulting $K$ value is 186.6, which is higher than the splashing threshold of 57.7 suggested by Mundo et al. [38]. A grid sensitivity analysis is performed. With two levels of mesh refinement, the grid with an effective grid resolution of 116 cells per initial drop diameter leads to a converged solution. Figure 6 shows the drop impact and the subsequent splashing phenomena. Right after contact with the solid surface, a thin liquid sheet is formed on the solid surface and moves radially outward. The sheet soon breaks up into small secondary drops. As the sheet breaks up at its perimeter into relatively large drops splashing is more prominent at the drop leading edge than at the trailing edge: a lower number of secondary drops us observed at the trailing edge, and their sizes are considerably smaller than those at the leading edge. The size distribution of the secondary drops is shown in Fig. 7. The secondary drop diameter is normalized using the diameter of the primary drop. Our simulation shows a qualitative agreement with the experiment. The numerical results are measured 59.1 $\mu$s after impact, but the time instant of the experiment results was not reported by Mundo et al. [38], which may contribute to the discrepancy.

### B. High-Speed Normal Impact on a Dry Surface

We simulate a water drop impact on a dry solid surface at a high impact speed. The water drop has a diameter of 100 $\mu$m and an initial velocity of 100 m/s. The resulting $K$ value is approximately 1300, the

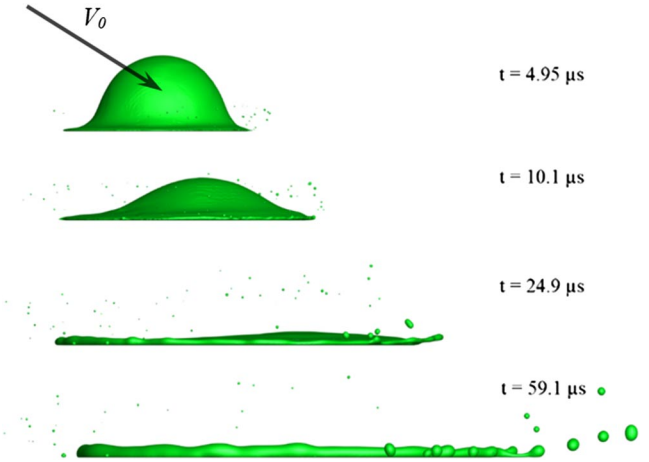


**Fig. 6 Simulation of oblique impact on dry solid surface, $D_0 = 100$ $\mu$m, $V_0 = 12$ m/s, $\alpha = 37$ deg, and $K = 186.6$. Secondary drops are larger on the upstream side.**

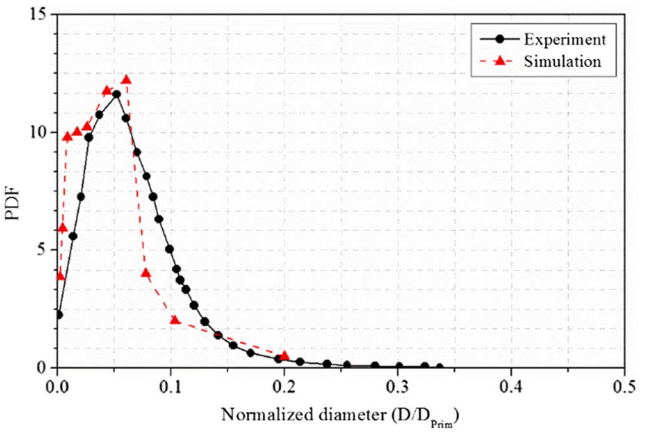


**Fig. 7 Comparison of size distribution of the splashed secondary drops between the simulation and the experiment. The time that the experiment data were taken was unknown (PDF, probability distribution function).**

Reynolds number $Re$ is 4000, and the Weber number $We$ is 28,000. The condition is similar to the drop impact on an aircraft in operational condition. With the increase of the $K$ value, the splashed secondary drops become smaller, which requires a fine mesh. A grid sensitivity analysis indicates that an effective grid resolution of 2800 cells per principle drop diameter gives convergent results. In the simulation, a six-level grid refinement is used. As shown in Fig. 8a, the majority of the splashed drops have a diameter of about 0.3% of the primary drop, and the total mass loss from splashing is 13.2% of the mass of the primary drop. Compared with the previous case of $K = 186.6$, the bandwidth of the size distribution function at $K = 1300$ is much narrower. Figure 8b shows the velocity distribution of the splashed secondary drops. The velocity of most secondary drops ranges from approximately 100 to 250 m/s, which is much higher than the initial impact velocity of 100 m/s. Figure 8c shows the shooting angle distribution of the secondary drops. Most shooting angles fall in the range between 0 and 40 deg. Note that a negative shooting angle means the secondary drop from an early stage of splashing is moving downward.

### C. Drop Impact on Thin Liquid Film

During flight, the wing surface is often covered with a liquid film from the impingement of previous drops. Therefore, understanding the drop impact on a wet surface is crucial for the water collection efficiency calculation. Experimental studies [39–42] revealed the threshold for drop splashing on a thin liquid film. For a stream of drops hitting the surface, Yarin and Weiss [40] proposed the following threshold velocity for splashing:

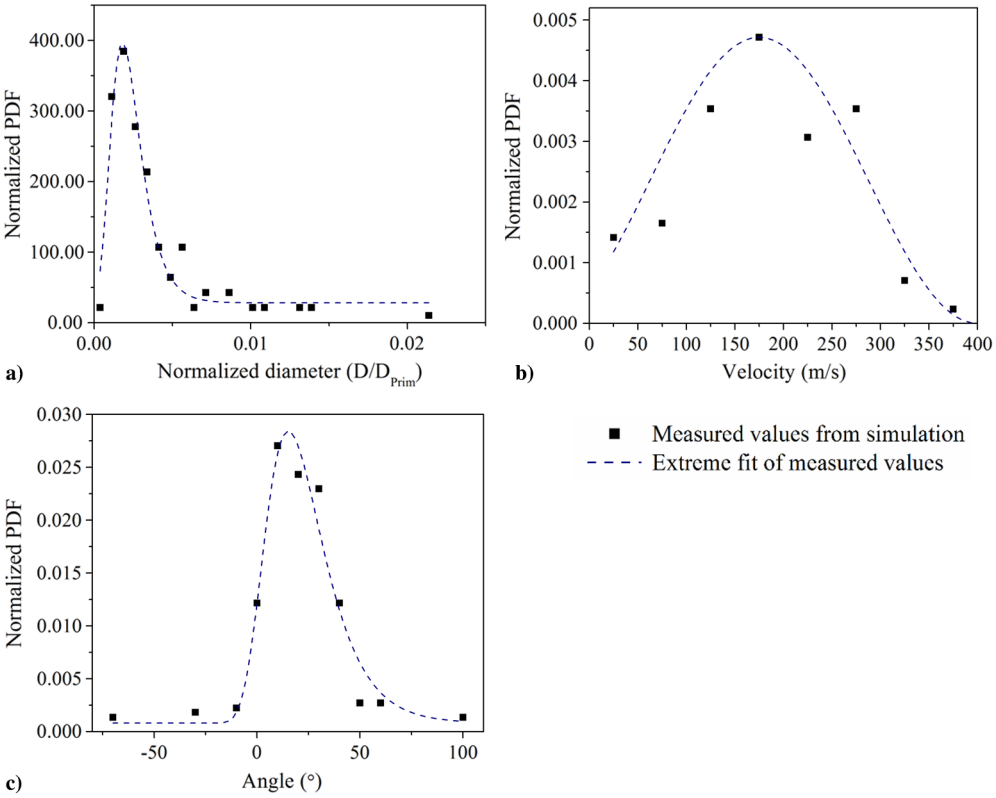


**Fig. 8 Normalized distributions of secondary drop diameter, velocity, and shooting angle for $K \approx 1300$.**

$$V_{0S} = 18\left(\frac{\sigma}{\rho}\right)^{1/4} \nu^{1/8} f^{3/8} \tag{15}$$

where $f$ is the frequency of incoming drops. For the single-drop problem, $f$ can be replaced with $V_0/D_0$. Their study showed that the drop diameter has no effect on the splashing threshold and the liquid film thickness is unimportant. Cossali et al. [41] proposed the following threshold for drop splashing on a thin liquid film with consideration of the film thickness:

$$K_S = 2100 + 5880\left(\frac{h}{D_0}\right)^{1.44} \quad \text{for } 0.1 < \frac{h}{D_0} < 1 \quad \text{and} \quad Oh > 0.007 \tag{16}$$

The threshold is valid for $h/D_0 > 0.1$. For $h/D_0 < 0.1$, Rioboo et al. [42] and Wang and Chen [39] suggested a threshold of $K_S \approx 400$.

Zhang and Hu [43] experimentally studied the water film over a NACA 0012 wing and measured the thickness of the water film. For wind speed ranges from 10 to 30 m/s, the measured film thickness ranges from approximately 2 to 40 $\mu$m, with thinner film for higher wing speed. The film thickness increases further downstream. For the operational flight speed, which is much higher than 30 m/s, the liquid film is supposed to be thinner than 2 $\mu$m.

Figure 9 shows the three-dimensional simulations of the normal impact of a single water drop onto a predefined thin water film. The initial diameter of the liquid drop $D_0$ is 100 $\mu$m, the normal impact velocity $V_0$ is 78 m/s, and the film thickness $h$ is 5 $\mu$m. The $K$ value is 667, which is greater than the threshold value $K_S$ of 400; and $V_0$ is greater than the threshold $V_{0S}$ of 28.8 m/s. The equivalent grid size is 288 cells per initial drop diameter with four-level adaptive mesh refinement. The simulation captures the formation and propagation of the lamellae. At the top of the lamella, the free rim becomes unstable and breaks up into multiple secondary drops. The calculated mass loss from splashing of this case is 26.56%, which is significantly higher than the splashed mass (13.2%) from the impact on a dry surface under the otherwise same operating conditions. Because the wing surface is wet during flight, the mass loss from wet surface splashing should be adopted for calculating the water collecting efficiency.

### D. Code Validation: Water Collection Efficiency Calculation for a Sphere

We validate the water collection efficiency calculated using our procedure with experimental measurement. The water collection efficiency calculation for a sphere body was performed experimentally by Lewis and Ruggeri [5]. The test body was a sphere of 15.04 cm in diameter, the MVD of spray generated by the nozzles was 18.6 $\mu$m, and the air speed was 80.8 m/s. Our three-dimensional simulation follows the same setup and is shown in Fig. 10. One-quarter of the sphere is simulated due to the symmetry of the problem. The symmetric boundary conditions are imposed at the surfaces shown in the red color, the inflow boundary condition is imposed at the surface shown in the blue color, and the outflow boundary conditions are imposed at the other three surfaces. Mesh are only refined for the regions containing the drop, and a three-level adaptive mesh refinement is used in this case. The equivalent grid resolution is 18 cells per drop diameter.

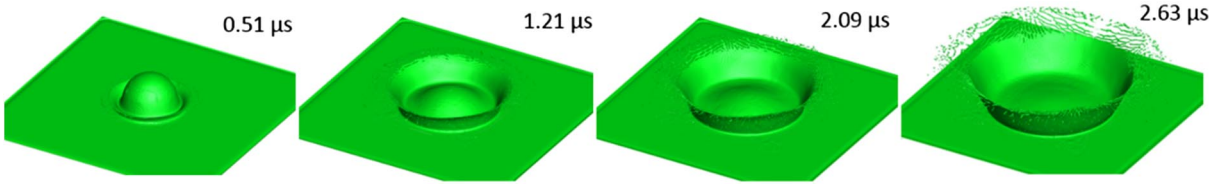


**Fig. 9 Drop impingement on a thin water film: $D_0 = 100$ $\mu$m, $h = 5$ $\mu$m, $V_0 = 78$ m/s, and $K = 667$.**

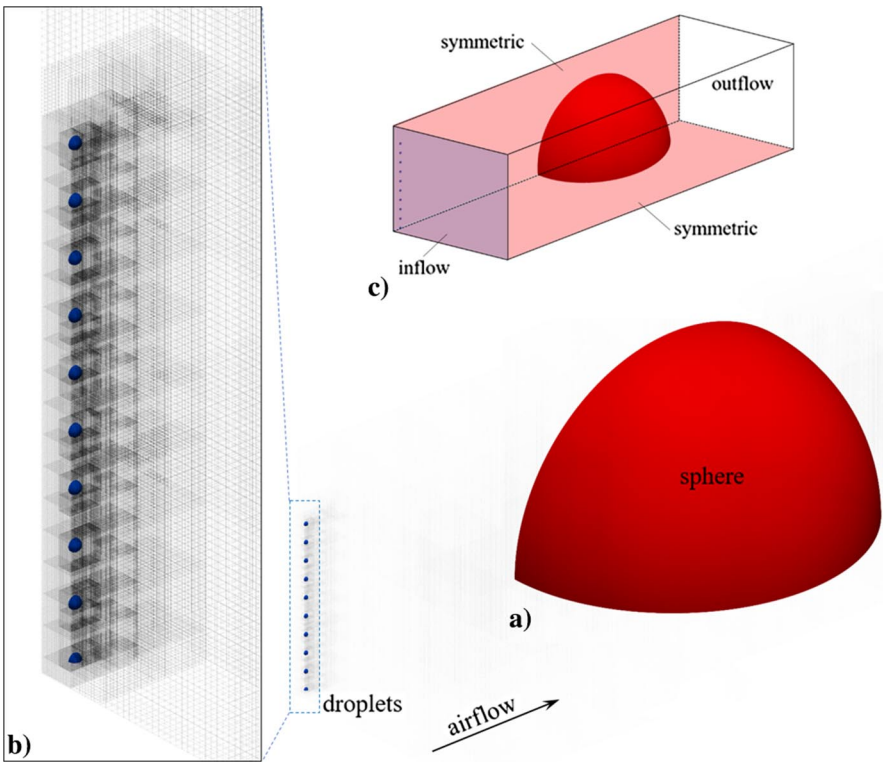


**Fig. 10 Three-dimensional simulation of drops impact on a sphere: a) simulation setup, b) zoomed-in view of drops with three-level adaptive mesh refinement, and c) boundary conditions. Blue = inflow; red = symmetric; and uncolored = outflow.**

The water collection efficiency calculation follows the procedure described in Fig. 5. In the first step, to obtain an MVD of 18.6 $\mu$m, a seven-bin drop distribution is used, as shown in Table 2. The drops are positioned at locations where the flow velocity is nearly parallel to the freestream velocity. When drops contact the airfoil, the water collection efficiency is calculated by considering the splashed mass. The impact limit is determined by the locations of the very top and bottom drops impacting onto the airfoil. Figure 11 compares the numerical results of water collection efficiency with the experimental data. Red triangles are the collection efficiency without considering the splashing effect. The blue squares are the collection efficiency with the consideration of the splashed mass. The numerical result of the collection efficiency better matches the experimental measurement when splashing is considered. The comparison results demonstrate that the splashing phenomenon is critical in calculating the collection efficiency.

### E. Water Collection Efficiency Calculation for an MS(1)-317 airfoil

Water collection efficiency for an MS(1)-317 airfoil is investigated. The experiment was conducted by Tan [3]. The airfoil chord was 0.914 m, the air speed was 78 m/s, the angle of attack (AOA) was 0 deg, and the MVD was 92 $\mu$m. In the experiment, a dye-tracer technique was used to obtain the water collection efficiencies and impact limits [4]. Dyed water drops were sprayed into the tunnel by nozzles, and the surface of the airfoil was covered with blotter paper to absorb the dye. Our simulation follows the same setup and is shown in Fig. 12. One narrow band of the airfoil is simulated, and drops are positioned at locations where the flow velocity is nearly parallel to the freestream velocity. Mesh are only refined for the regions containing the drop, and two-level adaptive mesh refinement is used in this case. The equivalent grid resolution is 12 cells per drop diameter. To obtain an MVD of 92 $\mu$m, a seven-bin drop distribution is used as shown in Table 3, and 21 drops of the same size are used for each group, as shown in Fig. 12. Our analysis shows that a further increase in the number of drops does not affect the collection efficiency.

**Table 2 Discretized drop distributions for MVD of 18.6 $\mu$m**

| Drop size, $\mu$m | Volume percentage, % |
|---|---|
| 5.77 | 5 |
| 9.67 | 10 |
| 13.21 | 20 |
| 18.6 | 30 |
| 25.48 | 20 |
| 32.36 | 10 |
| 41.29 | 5 |

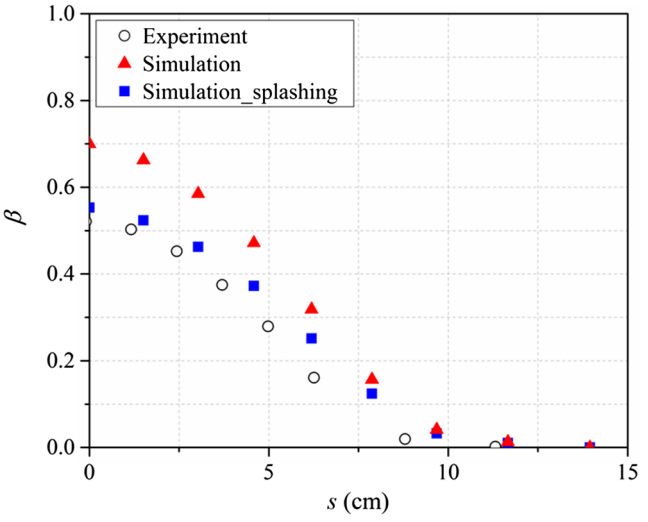


**Fig. 11 Water collection efficiency comparison between experiment and simulation.**

Figure 13 is the sliced view and shows the streamlines after drops impact on the airfoil surface. Unlike an existing icing code such as LEWICE, the interaction between the drops and air is fully coupled in our simulations. As shown in Fig. 13, the streamlines are clearly affected by the existence of drops, and the drops deform before impact due to the effect of surrounding air.

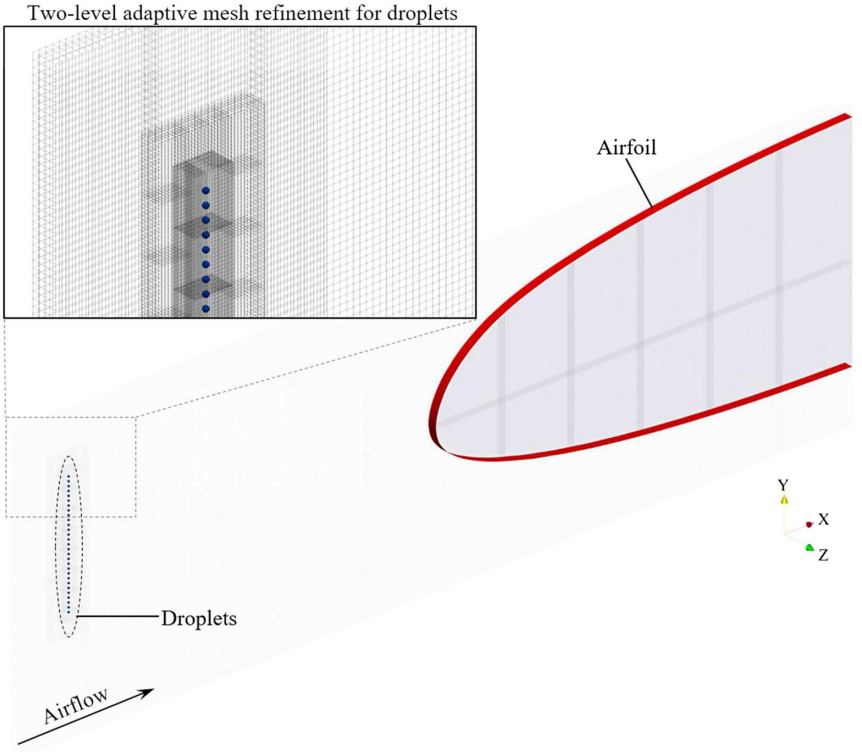


**Fig. 12 Three-dimensional simulation setup of drops impact on an MS(1)-317 airfoil. The zoomed-in view shows the two-level adaptive mesh refinement near the regions containing drops.**

**Table 3 Discretized drop distributions for MVD of 92 $\mu$m**

| Drop size, $\mu$m | Volume percentage, % |
|---|---|
| 29.14 | 5 |
| 48.88 | 10 |
| 66.74 | 20 |
| 94.0 | 30 |
| 128.78 | 20 |
| 163.56 | 10 |
| 208.68 | 5 |

The calculated water collection efficiency of each group is compared with LEWICE results in Fig. 14. Without drop splashing considered, our results are similar to the LEWICE results. For the group of the smallest drops (29.14 $\mu$m, cloud-sized drops), our simulation closely matches the LEWICE result. For large drops, LEWICE shows higher limits than our simulation. LEWICE is validated for drops for which the sizes are between 5 and 50 $\mu$m [44], and it assumes the drops are solid and spherical. The trajectory is calculated as a postprocessing in which the flow affects the drops but not the other way around. However, our numerical results show strong interaction between the air and water drops, which could potentially affect the predicted water collection efficiency and impingement limit.

For those drops that hit the wing, their water collection efficiency is further adjusted with the consideration of splashing. Figure 15 shows the combined $\beta$ result with the volume percentage of each drop size counted. The line with circles is the experimental data, the red dashed line is our simulation result without the splashing effect, the blue line shows our simulation with the splashing effect considered, and the black dotted line is the LEWICE result. The comparison clearly shows that LEWICE overestimates the impact limit, whereas our simulations with or without the splashing effect fit the experimental impact limit. Because drop splashing is only occurring near the leading-edge area, the splashing effect is negligible for a large impact angle.

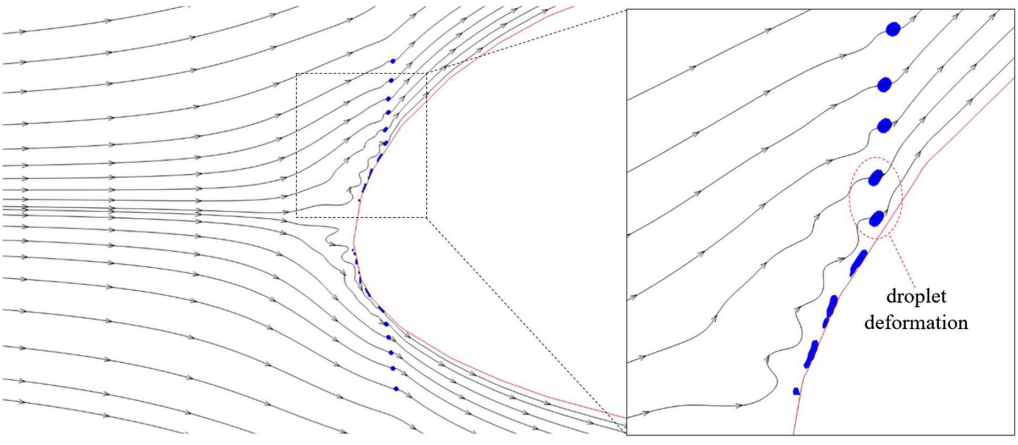


**Fig. 13 Altered streamlines and drop deformation due to interaction between drops and airflow.**

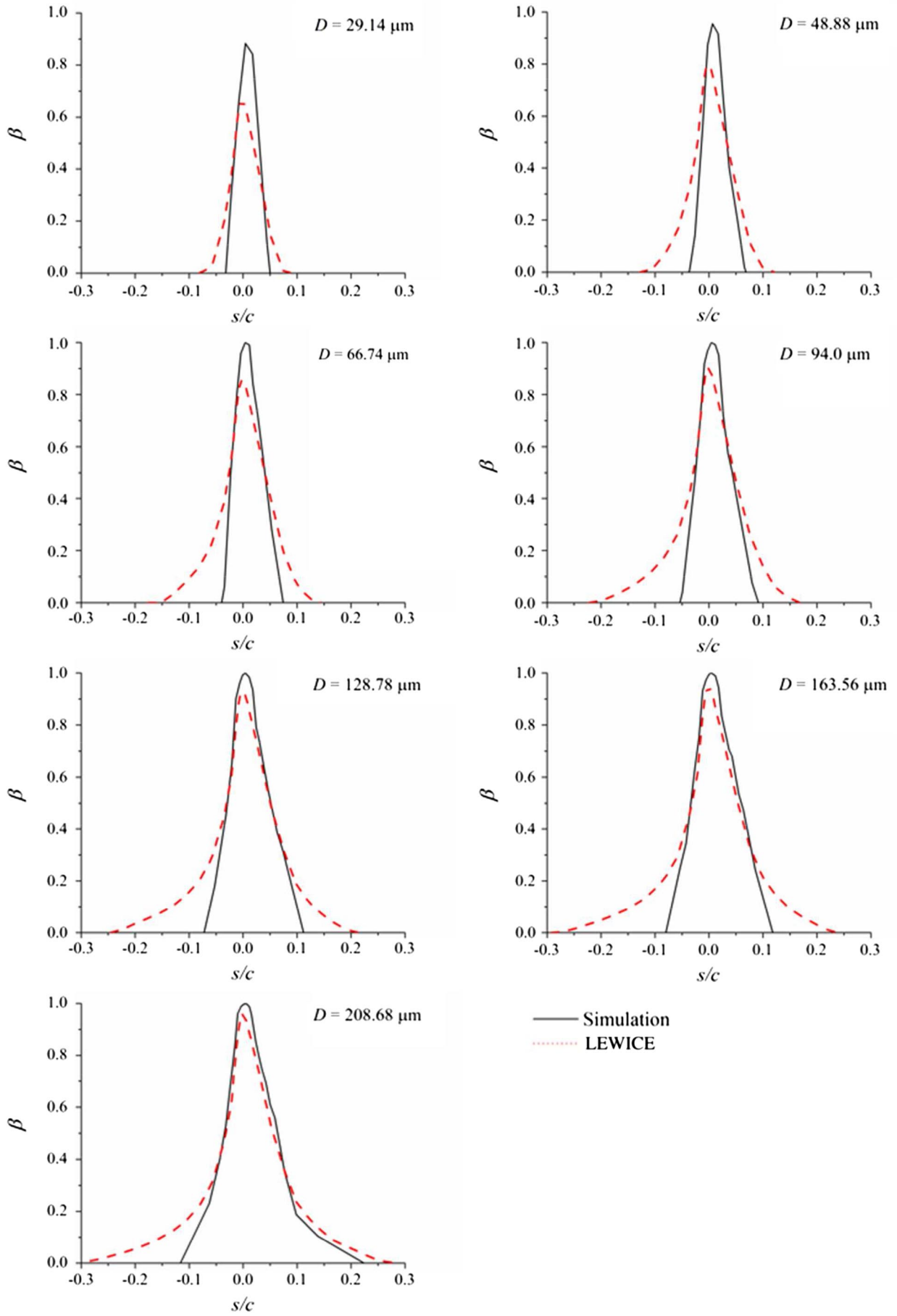


**Fig. 14 Water collection efficiencies of single-sized drops.**

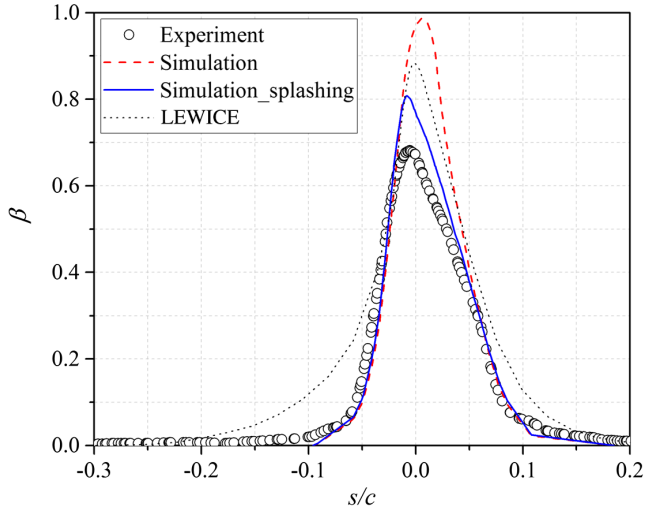


**Fig. 15 Water collection efficiencies comparison of experiment, simulations, and LEWICE.**

## IV. Conclusions

A numerical study was conducted to investigate the drop impingement phenomenon on dry and wet surfaces and to calculate the collection efficiency of water drops on an MS(1)-317 wing. The flowfield around the airfoil was described by solving Navier–Stokes equations. The drop impact on the surface and the subsequent phenomenon were captured directly in the simulations. The adaptive mesh refinement technique was employed to refine the mesh near regions of interest. The numerical code was first validated against an experiment of the drop impact on a dry surface, and good agreement was achieved. Simulations of the drop's impact on dry and wet surfaces were performed to study the mass loss from the drop splashing effect. Another validation case was conducted to calculate the water collection efficiency of a sphere body, and the numerical result agreed well with the experimental data. Lastly, the water collection efficiency of an MS(1)-317 wing was calculated. Compared with the experimental data, the simulation showed better agreement than LEWICE. LEWICE predicted well for cloud-sized drops but overestimated the impact limit for supercooled large drops.

The following important conclusions can be made from the present study:

1) Drop splashing leads to mass loss after impact, and splashing on the thin liquid film is found to have significantly more mass loss than on a dry surface. Neglecting the drop splashing effect may cause poor collection efficiency prediction.

2) Strong interaction between the water drops and air is observed. The streamlines of airflow are altered by drops, and the drops deform due to the effect of surrounding air.

## References

[1] Bragg, M. B., Gregorek, G. M., and Lee, J. D., "Airfoil Aerodynamics in Icing Conditions," *Journal of Aircraft*, Vol. 23, No. 1, 1986, pp. 76–81. doi:10.2514/3.45269

[2] Ranaudo, R. J., Batterson, J. G., Reehorst, A. L., Bond, T. H., and Omara, T. M., "Effects of Horizontal Tail Ice on Longitudinal Aerodynamic Derivatives," *Journal of Aircraft*, Vol. 28, No. 3, 1991, pp. 193–199. doi:10.2514/3.46012

[3] Tan, S. C., "A Tentative Mass Loss Model for Simulating Water Droplet Splash," *42nd AIAA Aerospace Sciences Meeting and Exhibit*, AIAA Paper 2004-0410, Jan. 2004.

[4] Gelder, T. F., Smyers, W. H., and Von Glahn, U., "Experimental Droplet Impingement on Several Two-Dimensional Airfoils with Thickness Ratios of 6 to 16 Percent," Lewis Flight Propulsion Lab. TN 3839, Cleveland, OH, 1956.

[5] Lewis, J. P., and Ruggeri, R. S., *Experimental Droplet Impingement on Four Bodies of Revolution*, Lewis Flight Propulsion Lab. TN 4092, Cleveland, OH, 1957.

[6] Papadakis, M., Elangonan, R., Freund, G. A., Jr., Breer, M., Zumwalt, G. W., and Whitmer, L., "An Experimental Method for Measuring Water Droplet Impingement Efficiency on Two- and Three-Dimensional Bodies," NASA CR 4257, 1989.

[7] Papadakis, M., Breer, M., Craig, N., and Liu, X., "Experimental Water Droplet Impingement Data on Airfoils, Simulated Ice Shapes, an Engine Inlet and a Finite Wing," NASA CR 4636, 1994.

[8] Papadakis, M., Hung, K. E., Vu, G. T., Yeong, H. W., Bidwell, C. S., Breer, M. D., and Bencic, T. J., "Experimental Investigation of Water Droplet Impingement on Airfoils, Finite Wings, and an S-Duct Engine Inlet," NASA TM 2002–211700, 2002.

[9] Morency, F., Beaugendre, H., Baruzzi, G. S., and Habashi, W. G., "FENSAP-ICE: A Comprehensive 3D Simulation Tool for In-flight Icing," AIAA Paper 2001-2566, 2001.

[10] Bourgault, Y., Habashi, W. G., Dompierre, J., and Baruzzi, G. S., "A Finite Element Method Study of Eulerian Droplets Impingement Models," *International Journal for Numerical Methods in Fluids*, Vol. 29, No. 4, 1999, pp. 429–449. doi:10.1002/(ISSN)1097-0363

[11] Potapczuk, M.G., Al-Khalil, K. M., and Velazquez, M. T., "Ice Accretion and Performance Degradation Calculations with LEWICE," NASA TM 105972, 1993.

[12] Wright, W. B., "Validation Results for LEWICE 3.0," AIAA Paper 2005-1243, 2005.

[13] Wright, W. B., "Further Refinement of the LEWICE SLD Model," 2006.

[14] Villedieu, P., Trontin, P., and Chauvin, R., "Glaciated and Mixed-Phase Ice Accretion Modeling Using ONERA 2D Icing Suite," *6th AIAA Atmospheric and Space Environments Conference*, AIAA Paper 2014-2199, 2014.

[15] Bilanin, A. J., "Proposed Modifications to Ice Accretion Icing Scaling Theory," *Journal of Aircraft*, Vol. 28, No. 6, 1991, pp. 353–359. doi:10.2514/3.46034

[16] Morency, F., Tezok, F., and Paraschivoiu, I., "Anti-Icing System Simulation Using CANICE," *Journal of Aircraft*, Vol. 36, No. 6, 1999, pp. 999–1006. doi:10.2514/2.2541

[17] Makkonen, L., Laakso, T., Marjaniemi, M., and Finstad, K. J., "Modeling Ice Accretion on Wind Turbines," *Wind Engineering*, Vol. 25, No. 1, 2001, pp. 3–21. doi:10.1260/0309524011495791

[18] Da Silveira, R. A., Maliska, C. R., Estivam, D. A., and Mendes, R., "Evaluation of Collection Efficiency Methods for Icing Analysis," *Proceedings of 17th International Congress of Mechanical Engineering*, 2003.

[19] Bragg, M.B., "Aerodynamics of Supercooled-Large-Droplet Ice Accretions and the Effect on Aircraft Control," *Proceedings of the FAA International Conference on Aircraft Inflight Icing*, Vol. 2, Springfield, VA. 1996, pp. 387–399.

[20] Bragg, M.B., "Aircraft Aerodynamic Effects due to Large Droplet Ice Accretions," AIAA Paper 1996-0932, 1996.

[21] Petty, K. R., and Floyd, C. D. J., "A Statistical Review of Aviation Airframe Icing Accidents in the US," *Proceedings of the 11th Conference on Aviation, Range, and Aerospace Hyannis*, 2004.

[22] "Airworthiness Standards: Transport Category Airplanes," Aeronautics and Space, Federal Aviation Administration Title 14, Federal Aviation Regulation Pt. 25, 2014, Amendment 140.

[23] "Large Aeroplanes," European Aviation SafetyAgency Certification Specification CS-25, 3 Dec. 2015, Amendment 16.

[24] Wright, W. B., and Potapczuk, M. G., "Semi-Empirical Modeling of SLD Physics," NASA TM-2004-212916, 2004.

[25] Rutkowski, A., Wright, W. B., and Potapczuk, M. G., "Numerical Study of Droplet Splashing and Re-Impingement," AIAA Paper 2003-0388, 2003.

[26] Li, G. B., Lian, Y. S., Guo, Y. S., Jemison, M., Sussman, M., Helms, T., and Arienti, M., "Incompressible Multiphase Flow and Encapsulation Simulations Using the Moment-of-Fluid Method," *International Journal for Numerical Methods in Fluids*, Vol. 79, No. 9, 2015, pp. 456–490. doi:10.1002/fld.v79.9

[27] Guo, Y., Lian, Y., and Sussman, M., "Investigation of Drop Impact on Dry and Wet Surfaces With Consideration of Surrounding Air," *Physics of Fluids*, Vol. 28, No. 7, 2016, Paper 073303. doi:10.1063/1.4958694

[28] Guo, Y., and Lian, Y., "High-Speed Oblique Drop Impact on Thin Liquid Films," *Physics of Fluids*, Vol. 29, No. 8, 2017, Paper 082108. doi:10.1063/1.4996588

[29] Dyadechko, V., and Shashkov, M., "Moment-of-Fluid Interface Reconstruction," Los Alamos National Lab. TR LA-UR-05-7571, Albuquerque, NM, 2005.

[30] Ahn, H.T., and Shashkov, M., "Multi-Material Interface Reconstruction on Generalized Polyhedral Meshes," *Journal of Computational Physics*,

Vol. 226, No. 2, 2007, pp. 2096–2132.
doi:10.1016/j.jcp.2007.06.033

[31] Dyadechko, V., and Shashkov, M., "Reconstruction of Multi-Material Interfaces from Moment Data," *Journal of Computational Physics*, Vol. 227, No. 11, 2008, , pp. 5361–5384.
doi:10.1016/j.jcp.2007.12.029

[32] Ahn, H.T., and Shashkov, M., "Adaptive Moment-of-Fluid Method," *Journal of Computational Physics*, Vol. 228, No. 8, 2009, pp. 2792–2821.
doi:10.1016/j.jcp.2008.12.031

[33] Jemison, M., Loch, E., Sussman, M., Shashkov, M., Arienti, M., Ohta, M., and Wang, Y., "A Coupled Level Set-Moment of Fluid Method for Incompressible Two-Phase Flows," *Journal of Scientific Computing*, Vol. 54, Nos. 2–3, 2012, pp. 1–38.

[34] Jemison, M., Sussman, M., and Arienti, M., "Compressible, Multiphase Semi-Implicit Method with Moment of Fluid Interface Representation," *Journal of Computational Physics*, Vol. 279, Dec. 2014, pp. 182–217.
doi:10.1016/j.jcp.2014.09.005

[35] Sussman, M., Almgren, A. S., Bell, J. B., Colella, P., Howell, L. H., and Welcome, M. L., "An Adaptive Level Set Approach for Incompressible Two-Phase Flows," *Journal of Computational Physics*, Vol. 148, No. 1, 1999, pp. 81–124.
doi:10.1006/jcph.1998.6106

[36] Sussman, M., "A Parallelized, Adaptive Algorithm for Multiphase Flows in General Geometries," *Computers and Structures*, Vol. 83, Nos. 6–7, 2005, pp. 435–444.
doi:10.1016/j.compstruc.2004.06.006

[37] Jiang, T.-S., Soo-Gun, O. H., and Slattery, J. C., "Correlation for Dynamic Contact Angle," *Journal of Colloid and Interface Science*, Vol. 69, No. 1, 1978, pp. 74–77.

[38] Mundo, C. H. R., Sommerfeld, M., and Tropea, C., "Droplet-Wall Collisions: Experimental Studies of the Deformation and Breakup Process," *International Journal of Multiphase Flow*, Vol. 21, No. 2, 1995, pp. 151–173.
doi:10.1016/0301-9322(94)00069-V

[39] Wang, A. B., and Chen, C. C., "Splashing Impact of a Single Drop onto Very Thin Liquid Films," *Physics of Fluids*, Vol. 12, No. 9, 2000, pp. 2155–2158.
doi:10.1063/1.1287511

[40] Yarin, A. L., and Weiss, D. A., "Impact of Drops on Solid-Surfaces-Self-Similar Capillary Waves, and Splashing as a New-Type of Kinematic Discontinuity," *Journal of Fluid Mechanics*, Vol. 283, Jan. 1995, pp. 141–173.
doi:10.1017/S0022112095002266

[41] Cossali, G. E., Coghe, A., and Marengo, M., "The Impact of a Single Drop on a Wetted Solid Surface," *Experiments in Fluids*, Vol. 22, No. 6, 1997, pp. 463–472.
doi:10.1007/s003480050073

[42] Rioboo, R., Bauthier, C., Conti, J., Voue, M., and De Coninck, J., "Experimental Investigation of Splash and Crown Formation During Single Drop Impact on Wetted Surfaces," *Experiments in Fluids*, Vol. 35, No. 6, 2003, pp. 648–652.
doi:10.1007/s00348-003-0719-5

[43] Zhang, K., and Hu, H., "An Experimental Study of the Wind-Driven Water Droplet/Rivulet Flows over an Airfoil Pertinent to Wind Turbine Icing Phenomena," *4th Joint US-European Fluids Engineering Summer Meeting*, Chicago, IL, 2014.

[44] Wright, W., *User's Manual for LEWICE Version 3.2*, QSS Group, Inc., Cleveland, OH, 2008, p. 15.